Journal of Power Sources 195 (2010) 204–213

Contents lists available at ScienceDirect

Journal of Power Sources

journal homepage: www.elsevier.com/locate/jpowsour

Performance analysis of a pressurized molten carbonate fuel cell/micro-gas turbine hybrid system

Aiguo Liu*, Yiwu Weng

School of Mechanical Engineering, Key Laboratory for Power Machinery and Engineering of Ministry of Education, Shanghai Jiao Tong Univ., 800 Dong Chuan Rd., Shanghai 200240, PR China

ARTICLE INFO

Article history:
Received 20 May 2009
Received in revised form 13 July 2009
Accepted 13 July 2009
Available online 21 July 2009

Keywords:
Pressurized molten carbonate fuel cell
Micro-gas turbine
Hybrid system
Part-load
Performance

ABSTRACT

This paper presents the work on the design and part-load operations of a hybrid power system composed of a pressurized molten carbonate fuel cell (MCFC) and a micro-gas turbine (MGT). The gas turbine is an existing one and the MCFC is assumed to be newly designed for the hybrid system. Firstly, the MCFC power and total system power are determined based on the existing micro-gas turbine according to the appropriate MCFC operating temperature. The characteristics of hybrid system on design point are shown. And then different control methods are applied to the hybrid system for the part-load operation. The effect of different control methods is analyzed and compared in order to find the optimal control strategy for the system. The results show that the performance of hybrid system during part-load operation varies significantly with different control methods. The system has the best efficiency when using variable rotational speed control for the part-load operation. At this time both the turbine inlet temperature and cell operating temperature are close to the design value, but the compressor would cross the surge line when the shaft speed is less than 70% of the design shaft speed. For the gas turbine it is difficult to obtain the original power due to the higher pressure loss between compressor and turbine.

1. Introduction

Molten carbonate fuel cell (MCFC) provides efficient means of producing electricity from fossil fuels with ultra low emissions. The high-temperature operating characteristics of MCFC provide the possibility of cogeneration with other types of power generator such as gas turbines. There are different system configurations for the combination of MCFC and MGT. One means is an ambient pressure system where the cell operates at a near ambient pressure [1]. The main advantage of this system is the selection of the MGT pressure independently of the cell pressure. Another means is called pressurized system where the MCFC is designed to operate at an elevated pressure. The pressurized oxidant is delivered to the MCFC and the outgoing high pressure gas drives the turbine [2,3]. The higher operating pressure guarantees higher cell performance. Some basic studies have concluded that a pressured system may have higher system efficiency over an ambient pressure system from a thermodynamic point of view if equivalent design parameters are assumed [4,5].

The simplest way to develop a hybrid system is to construct a system based on existing fuel cell or gas turbine and optimizes the system under given conditions [3,6–10]. The design of a hybrid system based on a commercially available gas turbine is more practical because the fuel cell power can be determined flexibly for the modular design of the fuel cell stack. The work about predicting system design and operations based on a commercial available gas turbine has ever been done. Different restricted issues have ever been considered to find the optimal power, such as the minimum electricity cost, maximum cell temperature, cathode inlet minimum percentage of CO_2, etc. At the same time different control methods have also been studied for the part-load operations of hybrid system. The performance characteristics of hybrid system at design and part-load conditions were compared and some useful conclusions have been drawn [3,10–15].

Little work has been done about the pressurized MCFC/MGT hybrid system on design and part-load performances based on commercially available gas turbine. In this study, the design of pressurized MCFC/MGT hybrid system using commercially available gas turbine was done at first. During the design procedure the important issue was the optimal matching between a chosen gas turbine and a pressurized MCFC module. The optimal fuel cell temperature was chosen as a limiting parameter in the determination of system power. Different control methods, including only fuel control, variable rotational speed gas turbine operation and air bypass control, were adopted for the realization of system part-load operation. The performance characteristics of hybrid system were compared and

* Corresponding author. Tel.: +86 13585630117; fax: +86 21 3420 6342.
E-mail address: liuaiguo119@yahoo.com.cn (A. Liu).

0378-7753/$ – see front matter © 2009 Elsevier B.V. All rights reserved.
doi:10.1016/j.jpowsour.2009.07.024

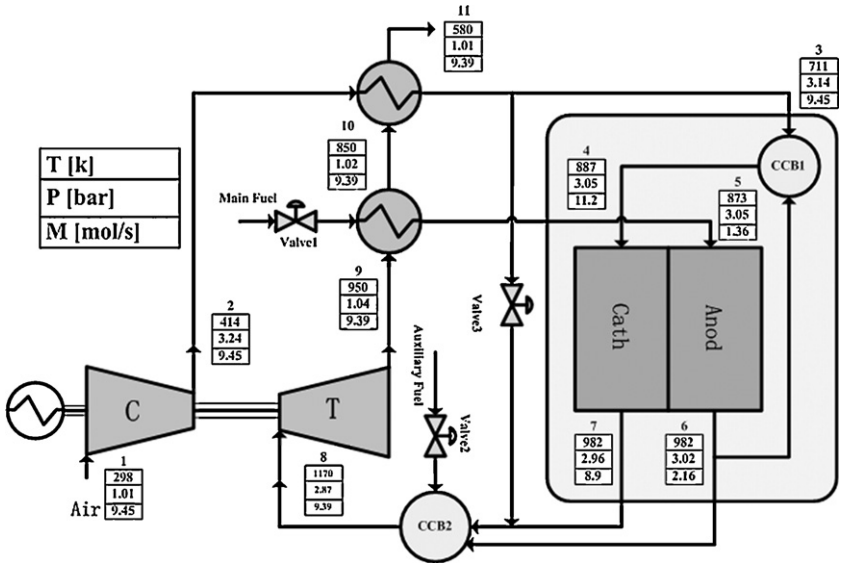

Fig. 1. Configuration of the pressurized MCFC/MGT hybrid system.

discussed under different control methods. The aim was to evaluate various part-load methods. This study presents the general analysis about pressurized MCFC/MGT hybrid system based on an exiting gas turbine which can provide the reference for the future work.

2. Approach

The pressurized MCFC/MGT hybrid system (HS) configuration is shown in Fig. 1. The hybrid system includes a pressurized MCFC stack, two heat exchangers (HE), two catalytic combustion burners (CCB1 and CCB2), an air compressor (C) and a gas turbine (T). The fuel is reformed using external reformer and the energy for reforming the hydrocarbon fuel is supplied by the waste heat from the system. The complete external reforming is assumed for all the simulations and the fuel compositions are H_2 73%, CO_2 8.3%, CO 6.5% and H_2O 12.2% according to the test results. The compressed air is heated through heat exchanger and then flows into the CCB1. In the CCB1 the air reacts with the residual fuels recycled from MCFC anode and then enters the cathode of the MCFC. The purpose of recycling anode exhaust is to increase the oxidant temperature and meet the CO_2 need in the electrochemical reaction. The anodic recycle ratio is 0.8 at the system design point which can meet the CO_2 need. The fuel to MCFC anode is main fuel and the fuel flow rate can be controlled by valve1. The main fuel is heated by the turbine exhaust and then enters the MCFC anode. The remaining fuel from the anode is combusted with the air and cathode exit gas in CCB1 and CCB2, respectively. The CCB2 also serves the purpose of separating the operation of the MCFC stack from that of gas turbine system, so that they are not thermally dependent on each other. For the present commercial gas turbine the turbine inlet gas temperature is 1173 K which is higher than the MCFC working temperature, and so additional fuel has to be provided. The fuel flow rate to CCB2 (auxiliary fuel) is analytically determined in order to achieve the turbine inlet temperature required and the flow rate can be controlled by valve2. The valve3 in Fig. 1 is used to bypass air for the part-load operation control.

2.1. Molten carbonate fuel cell model

The pressured MCFC model considered in this study is based on the co-flow planar kW class MCFC stack module and the electrolyte is $LiNaCO_3$ constructed by Shanghai Jiaotong University Fuel Cell Research Institute [16]. Increasing the number of multiple sub-stacks could modularly raise the MCFC power. To simplify the modeling, some reasonable assumptions are summarized as follows:

(1) Only H_2 is electrochemically oxidized.
(2) Constant Nusselt number.
(3) Adiabatic boundaries for the cell.

The model of MCFC consists of both electrochemical and thermal models [17]. In a MCFC, the electric power is generated through the following process:

$$\text{Anode}: H_2 + CO_3^{2-} \rightarrow CO_2 + H_2O + 2e^- \quad (1)$$

$$\text{Cathode}: CO_2 + \tfrac{1}{2}O_2 + 2e^- \rightarrow CO_3^{2-} \quad (2)$$

The relation between cell current density and voltage is written as follows:

$$i = \frac{E - V}{R_{\text{anod}} + R_{\text{cath}} + R_{\text{ir}}} \quad (3)$$

E given by the Nernst potential is the function of temperature and gas partial pressure in anode and cathode which can be regulated as follows:

$$E = E_0 + \frac{RT}{2F} \ln\left[\frac{P_{H_2,\text{anod}}(P_{O_2,\text{cath}})^{1/2}P_{CO_2,\text{cath}}}{P_{H_2O,\text{anod}}P_{CO_2,\text{anod}}}\right] \quad (4)$$

where E_0 is the ideal standard potential for the cell reaction, P is the gas partial pressure in anode and cathode.

The irreversible losses R_{anod}, R_{cath} at electrodes depend on temperature, pressure, partial pressure of gases H_2 at anode, CO_2 and O_2 at cathode, and some parameters related to electrodes and electrolytes. The cell internal resistance R_{ir} depends on the ionic conductivity of the electrolyte and electrical conductivity of the plates. The detailed description of the irreversible losses and parameters related with electrolyte can be found in [18].

Water–gas shift reaction (WGSR) will take place and reach to the equilibrium rapidly. An equilibrium-limited shift reaction rate expression, first order in carbon monoxide and with an arbitrarily high pre-exponential factor k_{WGSR} is given as [19]:

$$R_{\text{shift}} = k_{\text{WGSR}}p_{\text{anod,CO}}\left(1 - \frac{p_{\text{anod},CO_2}p_{\text{anod},H_2}}{k_{\text{shift}}p_{\text{anod,CO}}p_{\text{anod},H_2O}}\right) \quad (5)$$

where k_{shift} is the equilibrium constant which can be described as the function of temperature:

$$k_{shift} = \exp\left(\frac{4276}{T} - 3.961\right) \quad (6)$$

The thermal model accounts for mass, energy, momentum conservation principles and thermodynamic properties. In mass balance the water–gas shift reaction and electrochemical reaction are considered. Detailed gas thermal and transport properties such as density, specific heat capacity, thermal conductivity and dynamic viscosity should be considered for the accuracy of model [20].

The energy balance includes heat transfer and energy change, such as the electrical power and the enthalpy changes of the chemical and electrochemical reactions. Four energy balance equations are considered for accurately calculating the temperature profile in any relevant part in the cell. The thermal flux for interconnector and positive-electrolyte-negative (PEN) includes thermal conduction, thermal convection with gas and thermal radiation between them, while for the PEN the enthalpy fluxes associated with the flow of oxygen, carbon dioxide and hydrogen to the PEN structure and the flow of water and carbon dioxide from the PEN structure are also taken into account. Meanwhile, the thermal flux in the gas channel is convective from the solid parts and enthalpy fluxes associated with the species flow between PEN and gas channel. A detailed energy balance equations are shown as follows:

Anode channel:

$$\frac{\partial \rho_{anod} e_{anod}}{\partial t} = -\frac{\partial(\rho_{anod} u_{anod} C_{p,anod} T_{anod})}{\partial x} + \left[\sum_{j=H_2,H_2O,CO_2} \nu_{j,III} R_{III} H_j + k_{anod,PEN}(T_{PEN} - T_{anod}) + k_{anod,INTC}(T_{INTC} - T_{anod}) + (-\Delta H)_{shift} R_{shift}\right] \frac{1}{h_{anod}} \quad (7)$$

Cathode channel:

$$\frac{\partial \rho_{cath} e_{cath}}{\partial t} = -\frac{\partial(\rho_{cath} u_{cath} C_{p,cath} T_{cath})}{\partial x} + \left[\sum_{j=O_2,CO_2} \nu_{j,III} R_{III} h_j + k_{cath,PEN}(T_{PEN} - T_{cath}) + k_{cath,INTC}(T_{INTC} - T_{cath})\right] \frac{1}{h_{cath}} \quad (8)$$

PEN:

$$\frac{\partial T_{PEN}}{\partial t} = \frac{1}{\rho_{PEN} C_{P.PEN} \tau_{PEN}} \left\{ \begin{array}{l} \lambda_{PEN} \tau_{PEN} \dfrac{\partial^2 T_{PEN}}{\partial x^2} - \\ k_{anod,PEN}(T_{PEN} - T_{anod}) - \\ k_{cath,PEN}(T_{PEN} - T_{cath}) - \\ \displaystyle\sum_{j=H_2,H_2O,CO_2} \nu_{j,III} R_{III} h_j - \\ \displaystyle\sum_{j=O_2,CO_2} \nu_{j,III} R_{III} h_j - IU + \\ \left[\dfrac{\sigma(T_{INTC}^4 - T_{PEN}^4)}{1/\xi_{INTC} + 1/\xi_{PEN} - 1}\right] \end{array} \right\} \quad (9)$$

Interconnector:

$$\frac{\partial T_{INTC}}{\partial t} = \frac{1}{\rho_{INTC} C_{P.INTC} \tau_{INTC}} \left\{ \begin{array}{l} \lambda_{INTC} \tau_{INTC} \dfrac{\partial^2 T_{INTC}}{\partial x^2} - \\ k_{anod.INTC}(T_{INTC} - T_{anod}) - \\ k_{cath.INTC}(T_{INTC} - T_{cath}) - \\ \left[\dfrac{\sigma(T_{INTC}^4 - T_{PEN}^4)}{1/\varepsilon_{INTC} + 1/\varepsilon_{PEN} - 1}\right] \end{array} \right\} \quad (10)$$

where R_{III} is the reaction rate of electrochemical reaction which can be expressed as $R_{III} = i/2F$.

Finally a one-dimension distributed parameters MCFC model was developed. But it includes nonlinear partial differential equations which makes it difficult to obtain theoretical solutions. Here the volume–resistance (V–R) characteristic modeling technique is applied [21,22]. In the fluid system, each component can be treated as one of three types—volume module, resistance module and volume-resistance module. In the volume module the pressure losses is neglected and accumulating fluid based on the difference of flow rates. While in the resistance module the fluid has an obvious pressure loss which determines the flow rate of the component. The MCFC is such kind of component which have the qualities of both volume and resistance module. The modeling technique is based on the lumped parameter idea. In order to depict the distributed parameter objects, the component is divided into several control units. In each control unit there are two modules: volume module and resistance module. Based on the idea above the partial differential equations can be interchanged to ordinary differential equations and one set of equations for the fluid in the control section can be obtained.

The MCFC model developed here is for the smallest unit cell which is considered to be in the center of a large stack and no edge effects have been present. To produce a useful voltage, a MCFC consists of several repeating electrochemical cells in a module, connected in parallel or series and assembled to compose a stack. The performance of stack and single cell is different as the effects of edge. Some effects have been omitted and the simulation results were corrected with the kW class MCFC stack experimental results. Fig. 2 shows the comparison of polarization curve between experimental and calculated values for different operation pressure. Comparison of the simulation results with the experimental results shows good agreement with regard to the voltage losses.

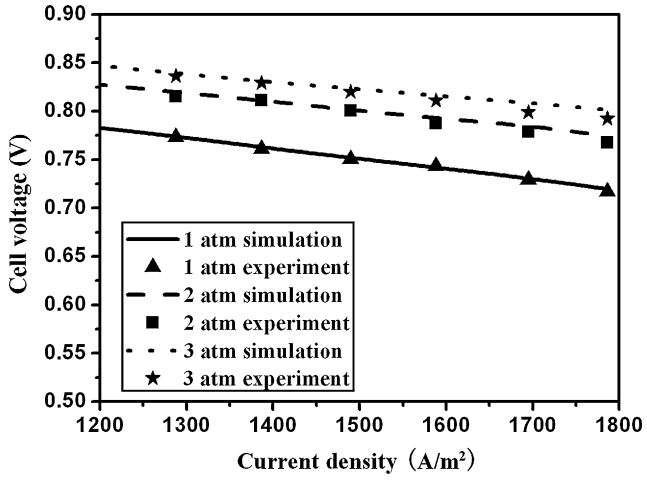

Fig. 2. Experimental and calculated values comparison.

2.2. Catalytic combustion burner model

In the catalytic combustion burner (CCB), the residual fuels from MCFC are burned away which increases the temperature of the gas. The following reactions are considered in calculating the exit gas temperature of the CCB:

$$CO + \tfrac{1}{2}O_2 = CO_2 + Q_{CO} \quad (11)$$

$$H_2 + \tfrac{1}{2}O_2 = H_2O + Q_{H_2} \quad (12)$$

Assuming that the process is adiabatic, the enthalpy of the reactants with combustion efficiency taken into account would be equal to the enthalpy of the products. Knowing the temperature of the reactants, the product temperature T_2 can be calculated by iteration as the properties of each product gas are temperature-dependent:

$$(\Delta H + Q_{CO} + Q_{H_2}) \cdot \varepsilon_{comb} = \sum_j m_j \int_{T_{std}}^{T_2} c_p dT \quad (13)$$

where the ΔH is the enthalpy change of reactions from the original status to the standard status, the combustion efficiency ε_{comb} was set conservatively at 98% at different load conditions, though it can be as high as 99.5%. The CCB pressure drop is kept for simplicity constant at partial load.

2.3. Heat exchanger model

The heat exchanger (HE) is a counter-flow one. The total amount of the heat exchanger heat loss is kept constant and independent with respect to the load. The air and gas side pressure drops are set to 3% and 6%, respectively at design conditions, and they are varied at partial load as a function of the mass flow and density according to the following relation:

$$\Delta P \cong \text{Const} \times \frac{m^2}{\rho} \quad (14)$$

as by the Darcy equation for turbulent flows, assuming a negligible variation of the fraction factor [12].

Setting the hot outlet pressure P_2 and enthalpy H_2, cold outlet pressure P_4 and enthalpy H_4 as the state variables, we can get the following equations based on the mass and energy balance [5,22].

$$\frac{dP_2}{dt} = \frac{(m_2H_2 - m_1H_1 - q_h)}{V_{ht}(1 - c_{p2}/R)} \quad (15)$$

$$\frac{dH_2}{dt} = \frac{(m_1H_1 - m_2H_2 + q_h) + (H_2 - H_2R/c_{p2})(m_2 - m_1)}{V_{ht}(\rho_2 - R\rho_2/c_{p2})} \quad (16)$$

$$\frac{dP_4}{dt} = \frac{(m_4H_4 - m_3H_3 + q_c)}{V_{cl}(1 - c_{p4}/R)} \quad (17)$$

$$\frac{dH_4}{dt} = \frac{(m_3H_3 - m_4H_4 - q_h) + (H_4 - H_4R/c_{p4})(m_4 - m_3)}{V_{cl}(\rho_4 - R\rho_4/c_{p4})} \quad (18)$$

where $q_{h,}$ q_c are the heat transfer between fluid (hot and cold) and the wall of the recuperator.

$$q_h = \alpha_h A_h (T_{12} - T_m) \quad (19)$$

$$q_c = \alpha_c A_c (T_m - T_{34}) \quad (20)$$

And the $T_{12} = (T_1 + T_2)/2$, $T_{34} = (T_3 + T_4)/2$ are the average value of inlet and outlet temperature, respectively.

T_m is the average wall temperature between the hot and cold side gas.

$$\frac{dT_m}{dt} = \frac{1}{C_{pm}M_m}(q_h - q_c) \quad (21)$$

Table 1
Specifications of the C30 gas turbine at design point.

Parameter	Value
Pressure ratio	3.20
Compressor isentropic efficiency (%)	80.00
Air flow rate (kg s^{-1})	0.31
Fuel flow rate (kg s^{-1})	0.0024
Turbine rotor inlet temperature (K)	1 173
Turbine isentropic efficiency (%)	90.00
Turbine exit temperature (K)	548
Turbine exit pressure (kPa)	103
Recuperator effectiveness (%)	90.00
Electric power generated (kW)	30
Electric efficiency (%)	26.0

2.4. Compressor and turbine models

Because of the matured technology of gas turbine and their commercial availability, a hybrid system with an off-the-shelf gas turbine has been constructed. The micro-gas turbine selected as the commercial available gas turbine is C30 from CAPSTONE. The gas turbine is a single-shaft micro-gas turbine equipped with a centrifugal compressor and a radial turbine. The design compressor pressure ratio is 3.2 and the turbine inlet temperature (TIT) is 1173 K. The design mass flow of 0.31 kg s^{-1} is assumed to produce roughly 30 kW power with an efficiency of 26% at ISO conditions. The performance of C30, based on its up-to-date specifications is summarized

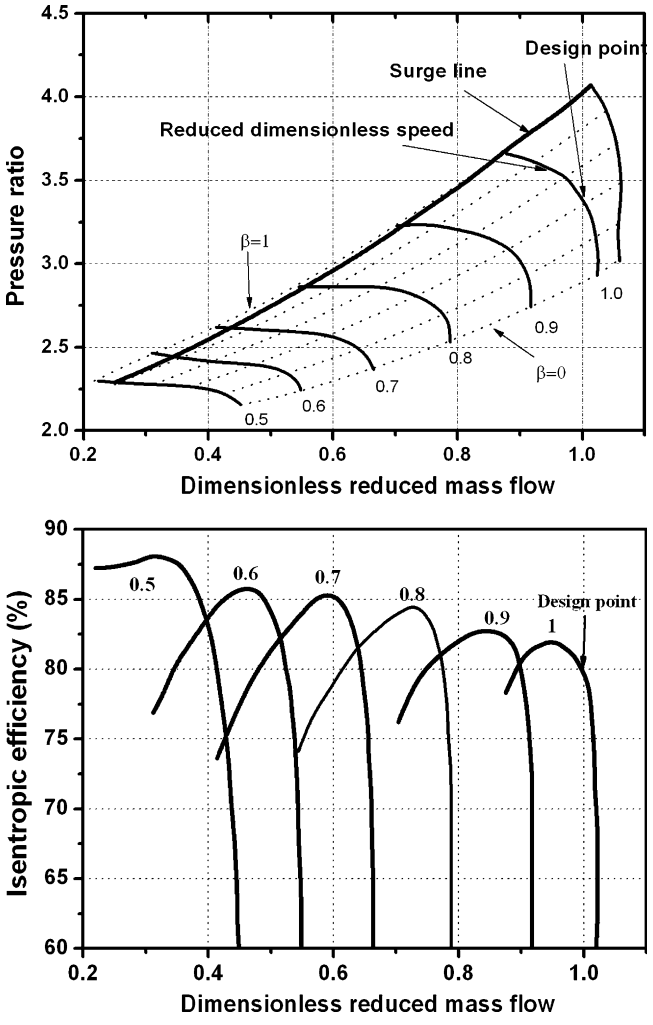

Fig. 3. Performance of compressor.

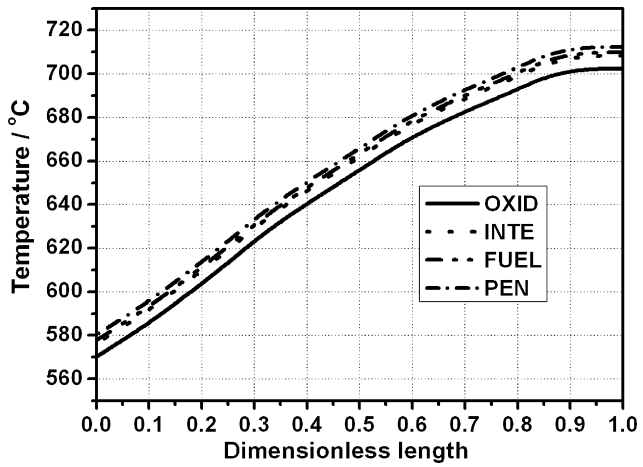

Fig. 4. Temperature distribution along flow direction.

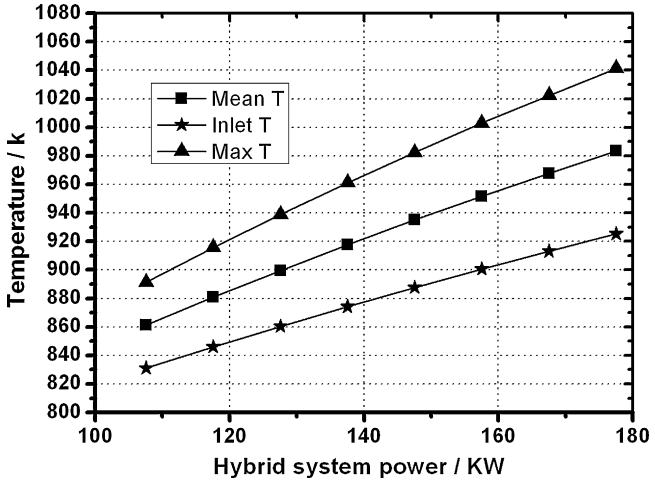

Fig. 5. Temperature with system power.

in Table 1. This single shaft gas turbine is capable of running at different shaft speed which generates higher flexibility for part-load operations.

The modeling of micro-gas turbine is possible by utilizing real steady state engine performance data [23]. In gas turbine cycles, the changed relationship between mass flow and pressure will cause a change in the operation point and efficiency. The features of a compressor can be described as functions of pressure ratio, reduced flow, reduced speed and efficiency. Performance maps are introduced for determination of the pressure and efficiency as a function of mass flow and shaft speed for the description of compressor. Fig. 3 shows the performance map of compressor. It is assumed that off-design thermodynamic and flow processes are characterized by a continuous progression along the steady-state performance curves.

The turbine model can be processed using a similar method.

The power output from the gas turbine is obtained by using the following equation:

(22)$W_{GT} = \eta_{gen}(\eta_t W_t - W_{comp}) - W_{aux}$where η_{gen} is the generator efficiency; η_t is the turbine mechanical efficiency; W_t, W_{comp} and W_{aux} are the turbine power, compressor power and auxiliary power, respectively.

Table 2
Specifications of MCFC/MGT hybrid system at design point.

Description	Value
MCFC	
Fuel flow rate (mol s^{-1})	1.365
Current density (A m^{-2})	1 500
Cell voltage (V)	0.82
Fuel utilization factor	0.8
Power (kW)	120
Efficiency (%)	49.8
Mean temperature (K)	930
GT	
Fuel flow rate (mol s^{-1})	0.022
Air flow rate (mol s^{-1})	9.45
Pressure ratio	3.2
Power (kW)	27.8
TIT (K)	1 173
HS	
Power (kW)	147.8
Efficiency (%)	58.53

2.5. Generator and valve models

The generator design efficiency of 95% is consistent with prototype test results. The inverter system efficiency has been set to 96%. The generator and inverter efficiency is reduced with the reduction of power. An efficiency decay of about 5% at 10% load was assumed to quantify the effects of auxiliary loss.

The valve is used for the control of fuel and gas flows. The valve is adiabatic and no fluid inertia is considered. Flow rate and molar composition of input and output are set equal at any load.

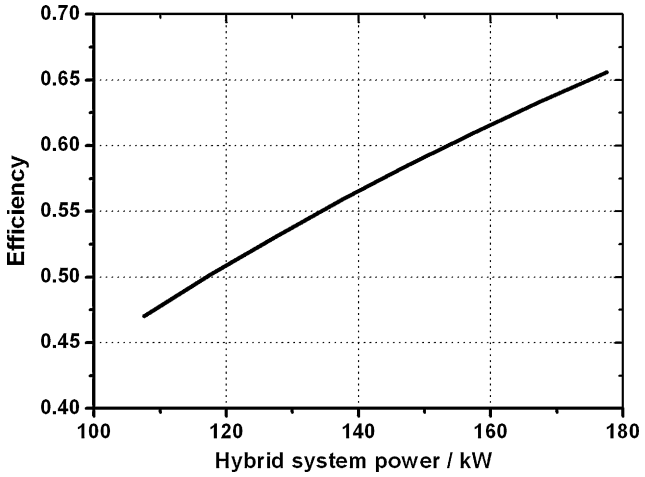

Fig. 6. Efficiency with system power.

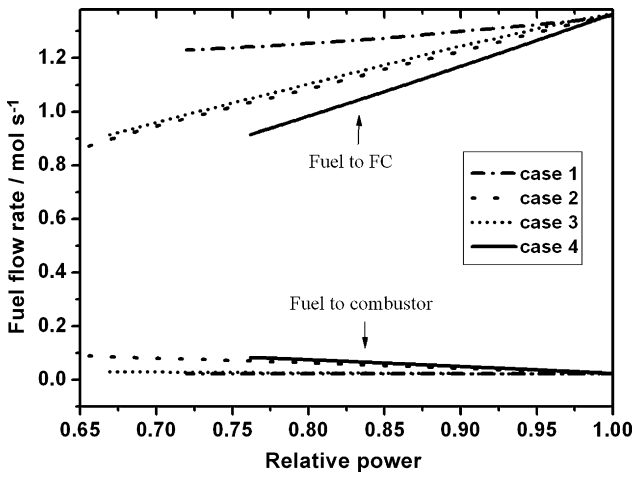

Fig. 7. Fuel flow rate to MCFC and CCB2 at part-load.

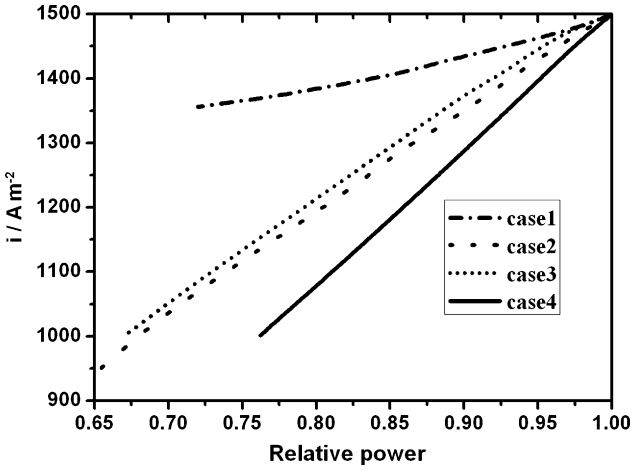

Fig. 8. Average current density change.

3. Results and discussion

3.1. Design point definition

The efficiency of MCFC is higher than that of micro-gas turbine. Since the micro-gas turbine has been selected the system efficiency of hybrid system could be raised by increasing the MCFC power. But some restricted issues should be considered for the decision of system power [3,10,15].

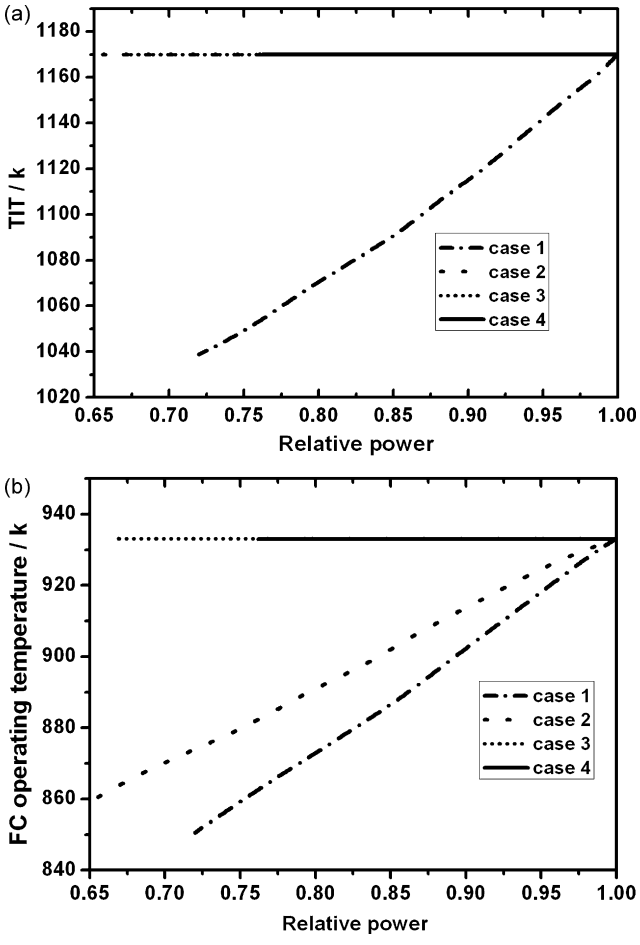

Fig. 9. Temperature at part-load: (a) TIT; (b) MCFC operation temperature.

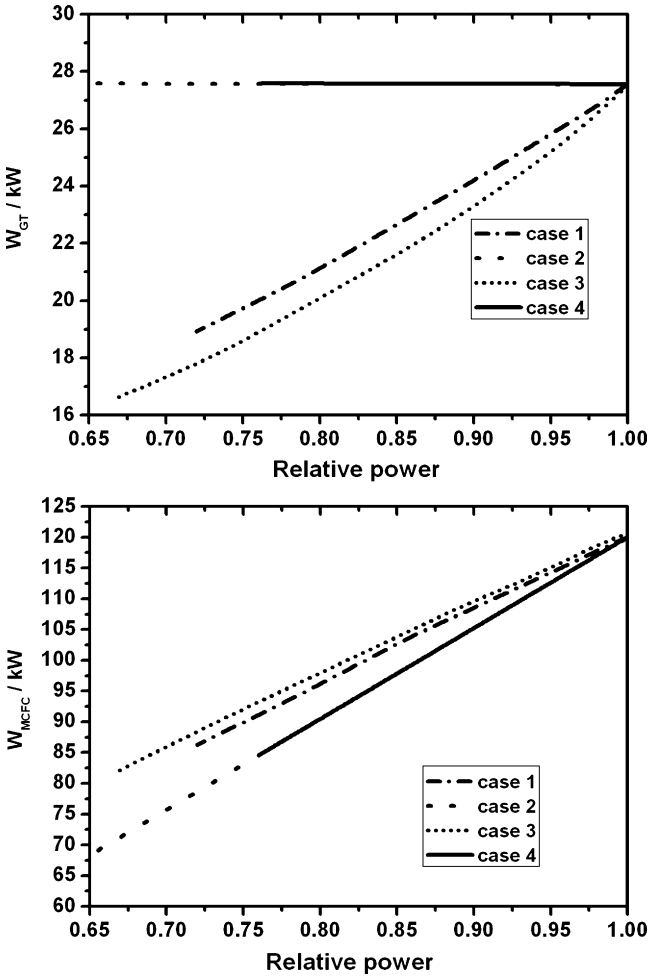

Fig. 10. MCFC and gas turbine power.

In this paper the restricted issue considered is the fuel cell operation temperature. The stack operating temperature should be greater than 853 K (580 °C) in order to guarantee the molten condition of the carbonate and less than 973 K (700 °C) for avoiding the increased electrolyte loss from evaporation and material corrosion. The local temperature distributions along the flow direction can be predicted based on the one-dimension distributed parameters MCFC model. The temperature profiles of the fuel channel, oxidant channel, interconnector and PEN structure are presented in Fig. 4 for one condition. As can be seen the temperature will increase along the gas flow direction owing to the heat accumulation released by the electrochemical and shift reactions. The maximum temperature occurs at the outlet. The fuel cell temperature used to restrict the output power is the average of inlet and maximum temperature of PEN structure.

The predicted fuel cell temperature and system efficiency are shown in Figs. 5 and 6. As can be seen the temperature and system efficiency were raised proportionally to the increase of MCFC power. Since the air supply is fixed by the selected gas turbine, the temperature of fuel cell would rise caused by the reduction of the oxidant supply to each MCFC with the increase in number of MCFC. The efficiency of MCFC is higher and it will increase with the temperature, so the system efficiency increases as the temperature and MCFC power increase.

While considering the performance of MCFC in different temperature 930 K was chosen to the favorite temperature. Based on the selected condition, the total system power is 147.8, 120 kW

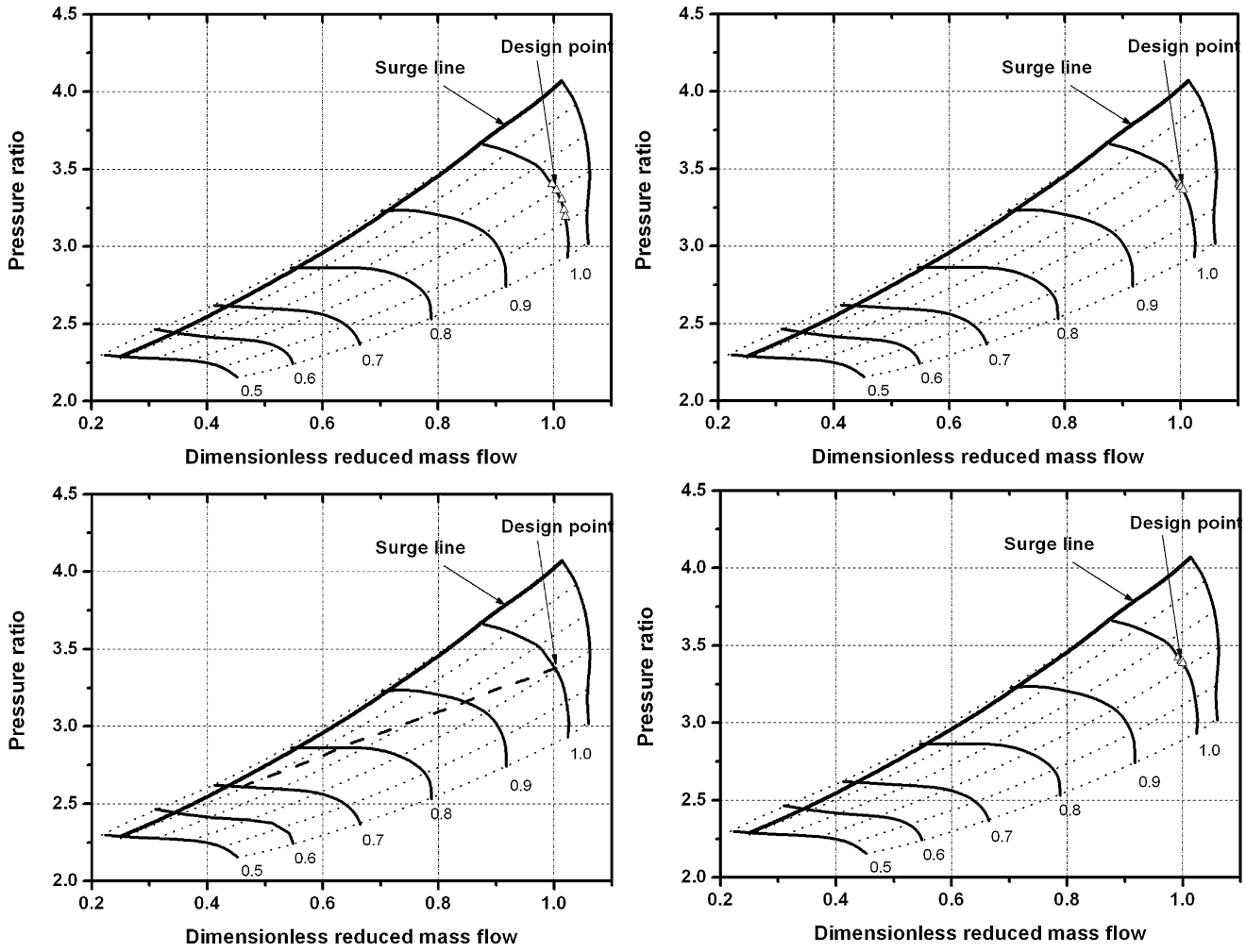

Fig. 11. Gas turbine compressor operational line in the compressor map.

from the stack and 27.8 kW from the gas turbine. The MCFC stack includes 3600 single cells and the total effective area is 100 m^2. The geometry of stack is based on an active area of single cell per bipolar array plate of 17 cm × 17 cm and the height is 0.4 cm for each cell. There are 900 single cells in each stack and the four stacks are assembled in parallel. The fuel feed and oxidant feed are divided into equal streams which flow in parallel through the stack.

The efficiency of whole plant is calculated as the ratio between the net power produced and the LHV of the feeding fuel, while the fuel cell efficiency is the ratio between the power supplied by the stack alone and the LHV of the fuel supplied to the fuel cell. According to the calculation the efficiencies of hybrid system and MCFC were 58.5% and 49.8, respectively, and the parameters for each node at design condition were shown in Fig. 1. The HS efficiency is lower compared with the references [3,9,10], in which the systems are designed based on an exiting SOFC and MCFC. This is because some fuel should be added into the combustor in front of turbine to meet the TIT for the lower operating temperature of MCFC. In comparison with the power ratio of the system designed based on MCFC in [3], the power ratio MCFC module and the gas turbine is higher in this system as the TIT is high. The current density of SOFC is higher than MCFC, so the numbers of single cell and effective area of stack are higher than SOFC described in [9,10] if the output power is the same. The output power of gas turbine is less than the original one though the TIT and compression ratio can be maintained as the design value. This is because the pressure loss caused by the components between compressor and turbine. The performance data representing the design point conditions of the pressurized MCFC/MGT hybrid system based on the C30 gas turbine is shown in Table 2.

3.2. Off-design analysis

When the power demand from the MCFC/MGT hybrid system is reduced, the system must be operated at part-load conditions. Various control methods can be considered for part loading the hybrid system. Adjusting the fuel supply is the general one, but some research results conclude that the simultaneous control of air and fuel supplies provides better part-load performance.

Different control methods can be adopted for the change of the air supplied to fuel cell, such as variable rotational speed control, variable inlet guide vane control and the HE discharge air bypass control [24,25]. Variable inlet guide vane control is mainly used in heavy gas turbine. So in this paper the part-load control methods for the pressurized MCFC/MGT hybrid system includes only fuel control, variable rotational speed with fuel control and air bypass with fuel control. Details of each control methods are described as different case as follows:

Case 1. Varying the main fuel (regulating valve 1).

Case 2. Varying the main fuel and auxiliary fuel simultaneously to keep the TIT as the design value (regulating valve 1 and valve 2).

Case 3. Varying the main fuel and auxiliary fuel simultaneously to keep the TIT and fuel cell operating temperature as the design value with variable speed gas turbine operation (regulating valve 1, valve 2 and rotational speed).

Case 4. Varying the main fuel and auxiliary fuel simultaneously to keep the TIT and fuel cell operating temperature as the design value with air-bypass model (regulating valve 1, valve 2 and valve 3).

The fuel flow rate to MCFC stack and CCB2 is shown in Fig. 7 for different control methods. The fuel flow rate to MCFC stack is decreased in all control method which is the main cause of the reduced power output of the hybrid system as the MCFC stack is the main power output source. Auxiliary fuel to CCB2 is necessary in the Cases 2–4. The amount of auxiliary fuel is analytical calculated to meet the requirements of component matching and to achieve system thermal and mass balance. In Cases 2 and 4 the auxiliary fuel to CCB2 is increased, while the amount in Case 3 is nearly constant which is because the variable speed turbine operation can decrease the amount of air.

Fuel utilization is an important performance parameter because it will determine whether or not the whole system is stably operating. Here the PID control technique is adopted to keep the fuel utilization constant through adjusting the operating voltage. The operating voltage through the cell is considered a constant as the electrode is good conductor, while the current density is changed along the flow direction because it is related with temperature and compositions. Here the average current density is adopted for the performance analysis of MCFC and the change of average current density for different control methods is shown in Fig. 8. The reduction of fuel flow rate will cause the decrease of current density according to the electrochemical model. The operating voltage will decrease in Cases 1 and 2 due to the reduction of MCFC operating temperature, while it will increase in Cases 3 and 4 because of the impact of temperature, current density and fuel utilization. The anodic recycle ratio is kept constant for part-load operation which can guarantee a sufficient CO_2 to the cathode.

The lowest part-load operation is limited by the current density and MCFC operating temperature. The current density is limited in the range of 100–200 mA cm^{-2}, and the MCFC operating temperature is limited between 853 and 973 K.

The MCFC operating temperature and TIT are shown in Fig. 9. As shown in Fig. 7, additional fuel is supplied to the gas turbine with the reduction of power generation for Cases 2–4. These cases describe the TIT is constant with the change of produced system power as shown in Fig. 9(a). The impossibility of reducing the air flow rate in Cases 1 and 2 results in an excessive cooling of stack. Especially in Case 1 the stack inlet temperature declines with the TIT which limits the reducing of power below 72% of the design point considering the operating limit (T_{min} > 853 K). On the other hand, due to the simultaneous control of supplied air and fuel to the MCFC stack in Cases 3 and 4 by variable rotational speed (Case 3) and air bypass (Case 4), both fuel cell operating temperature and TIT were maintained as design value at part-load conditions.

Fig. 10 shows the power from gas turbine and fuel cell at part-load conditions. In Case 1 the turbine rotational speed is constant and the TIT decreases which causes the output power decrease. In Cases 2 and 4, the air flow rate is constant and the TIT is kept near the design value which causes the gas turbine power as design value. While in Case 3, the variable rotational speed operation of gas turbine reduces air flow rate which causes the reduction of gas turbine power at part-load condition. The MCFC stack power is the function of cell voltage and current density. The current density will decrease with the reduction of fuel flow rate which causes the reduction of fuel cell power.

The hybrid system operational range in the compressor characteristic map is shown in Fig. 11 for different control methods. At constant compressor shaft speed (Cases 1, 2 and 4), the operational range is rather small. And thus the air flow rate is almost constant. In Case 1 the MCFC stack operating temperature and TIT decrease which makes the compressor surge margin increase at part-load condition. In Cases 2 and 4 the TIT is almost constant, which causes the pressure and air mass are also almost constant. The compressor surge will not occur at constant rotational speed operation. In Case 3, with decreased shaft speed, the operational points on a constant speed line continuously approach the surge line. At 70% of the design shaft speed, the compressor would almost cross the surge line. The compressor surge limit will be another limited parameter for the part-load operation besides the operating temperature and current density.

The efficiency of MCFC and hybrid system is shown in Fig. 12. The decrease in stack power is due mainly to the reduced fuel flow rate and hence the reduced current density of the cell. In MCFC stack the electrical efficiency can be still high when the system operates at part-load conditions because its efficiency is a function of cell voltage and fuel utilization.

In Cases 1 and 2, the reduction of air flow rate to MCFC is impossible which results in an excessive cooling of the stack. The fuel supply to fuel cell will increase compared with the single operation of MCFC at the same part-load condition. At the same time the reduction of operation temperature can cause an increase in electrical losses. So the efficiency of MCFC will decrease in these cases. In Cases 3 and 4 the fuel cell operates more efficiently at

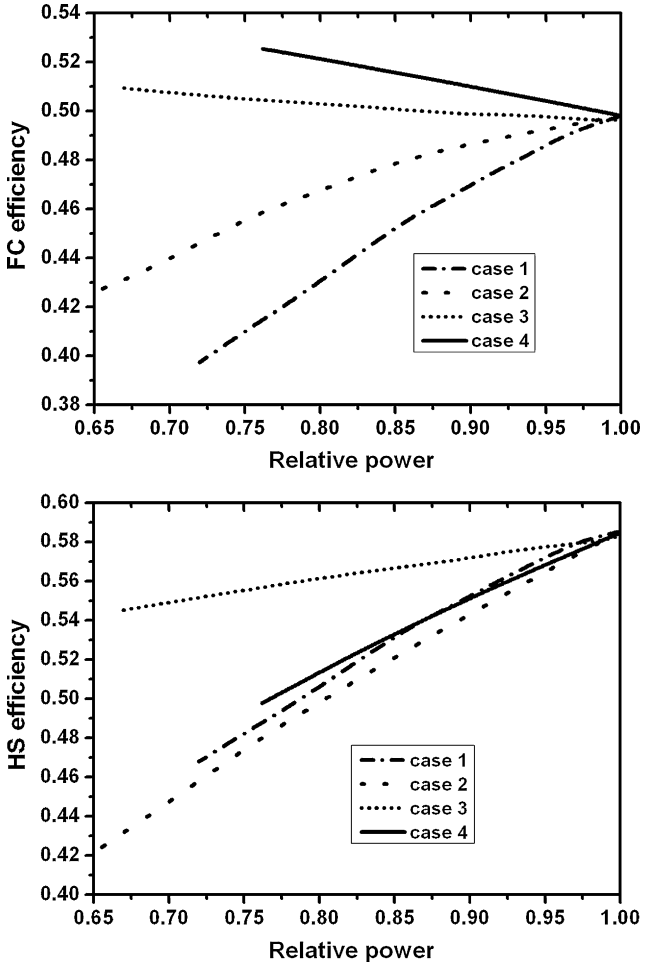

Fig. 12. Efficiency of MCFC and hybrid system.

part-load as the air flow to MCFC was reduced which causes the operation temperature is maintained at the design value. The cell voltage becomes higher because of the operating temperature and current density. In the view of the hybrid system efficiency the Case 3 is the highest. This is due to the simultaneous positive influence of MCFC stacks off-design behavior and gas turbine variable speed control. The turbine rotational speed is kept constant in Cases 1, 2 and 4, the air flow rate little changes which is a limit for hybrid system efficiency at part-load condition since more fuel is used in the CCB2. The efficiency of Case 2 is the lowest because more fuel should be directly used in the CCB2 to improve the turbine inlet temperature. The lower gas turbine efficiency would cause the hybrid system efficiency decrease.

4. Conclusions

The performance of pressurized MCFC/MGT hybrid system based on a commercially available micro-gas turbine has been analyzed. The system power has been discussed considering the allowable cell temperature, and the system design point conditions were presented. The efficiency of hybrid system is 58.5% which is lower than the system structure with a pressured SOFC and the system designed based on an exiting MCFC because of the characteristics of MCFC and micro-gas turbine.

The performance of system and components were analyzed for part-load operations under different control methods considering the limited parameters. The only fuel control method (Case 1) is the simplest, but it causes the lower efficiency and operation range because the TIT and cell operating temperature both decrease. In Case 2 the TIT is kept constant which enlarges the operation range but further decreases the efficiency. The variable rotational speed control method (Case 3) provides the best performance due to the TIT and cell temperatures are maintained as the design value. But the compressor operation will cross the surge line at lower load. For the air bypass control method (Case 4), the efficiency and part-load operation ranges are lower than the rotational speed control method but the compressor works near the design point and the surge will not happen.

Nomenclature

A	effective heat transfer area, m^2
C_p	specific heat capacity, $kJ\,kg^{-1}\,K^{-1}$
e	specific internal energy, $kJ\,kg^{-1}$
E	reversible potential, V
E_0	ideal standard potential, V
F	Faraday constant
h	channel height, m
H	specific enthalpy, $kJ\,kg^{-1}$
i	current density, $A\,m^{-2}$
$k_{anod,PEN}$ $k_{anod,INTC}$	anode channel heat transfer coefficient, $kJ\,m^{-2}\,s^{-1}\,K^{-1}$
$k_{cath,PEN}$ $k_{cath,INTC}$	cathode channel heat transfer coefficient, $kJ\,m^{-2}\,s^{-1}\,K^{-1}$
m	mass flow rate, $kg\,s^{-1}$
M_m	mass of the metal wall of the heat exchanger, kg
P	pressure, bar
Q	reaction enthalpy, $kJ\,mol^{-1}$
R	universal gas constant, $kJ\,kg^{-1}\,K^{-1}$
R_{anod}	anode irreversible loss, $\Omega\,cm^{-2}$
R_{cath}	cathode irreversible loss, $\Omega\,cm^{-2}$
R_{ir}	internal resistance, $\Omega\,cm^{-2}$
T	temperature, K
u	velocity, $m\,s^{-1}$
V	output voltage, V
V_{ht}	hot side volume of heat exchanger, m^3
V_{cl}	cold side volume of heat exchanger, m^3
W	power, kW

Greek symbol

ΔH	enthalpy change of reaction, $kJ\,kg^{-1}$
α	convective heat transfer coefficient, $kW\,m^{-1}\,K^{-1}$
ε	emissivity
η	efficiency
λ	thermal conductivity, $kJ\,m^{-1}\,s^{-1}\,K^{-1}$
ρ	density, $kg\,m^{-3}$
σ	Stefan–Boltzmann constant, $W\,m^{-2}\,K^{-4}$
τ_{INTC},τ_{PEN}	thickness of interconnector and PEN structure, m
$\nu_{j,III}$	stoichiometric coefficient of component j in electrochemical reaction
ξ_{comb}	combustion efficiency

Subscripts and superscripts

anod	anode channel
cath	cathode channel
c	cold side of heat exchanger
comp	compressor
comb	combustor
gen	generator
GT	gas turbine
h	heat side of heat exchanger
ir	internal resistance
INTC	interconnector
j	component
m	metal wall of heat exchanger
PEN	PEN structure
stad	standard condition
t	turbine
WGSR	water–gas shift reaction

Acknowledgment

This project was supported by National Natural Science Foundation of China (NSFC) under the contract no. 90610019.

References

[1] K.S. Oh, T.S. Kim, J. Power Sources 158 (2006) 455–463.
[2] B. Sam Kang, J.-H. Koh, H.C. Lim, J. Power Sources 108 (2002) 232–238.
[3] P. Bedont, O. Grillo, A.F. Massardo, J. Eng. Gas Turbines Power 125 (2003) 986–993.
[4] S.K. Park, T.S. Kim, J. Power Sources 163 (2006) 490–499.
[5] H. Zhang, S. Weng, M. Su, Evaluation of Topping and Bottoming Cycle Hybrid power Plants with mcfc-micro Turbine, ASME Paper GT2004-53397, 2004.
[6] H. Ghezel-Ayagh, J.M. Daly, Z.H. Wang, Advances in Direct fuel cell/gas Turbine Power Plant, ASME Paper GT2003-38941, 2003.
[7] U. Desideri, P. Lunghi, S. Ubertini, Feasibility and Performance of an Ambient Pressure MCFC Combined with a Commercial gas turbine, ASME Paper GT2002-30650, 2002.
[8] P. Lunghi, R. Bove, U. Desideri, J. Power Sources 118 (2003) 108–117.
[9] S.K. Park, K.S. Oh, T.S. Kim, J. Power Sources 170 (2007) 130–139.
[10] T.W. Song, J.L. Sohn, T.S. Kim, S.T. Ro, J. Power Sources 158 (2006) 361–367.
[11] F. Calise, A. Palombo, L. Vanoli, J. Power Sources 158 (1) (2006) 225–244.
[12] S. Campanari, J. Eng. Gas Turbines Power 122 (2000) 239–246.
[13] G.C. Karvountzi, P.F. Duby, Part Load Strategies of a Multi-MW Molten Carbonate Fuel Cell Gas Turbine Hybrid System, ASME Paper, GT 2007-27119, 2007.
[14] F. Yoshiba, Y. Izaki, T. Watanabe, J. Power Sources 137 (2004) 196–205.
[15] W.L. Lundberg, S.E. Veyo, M.D. Moeckel, ASME J. Eng. Gas Turbine Power 125 (2003) 51–58.
[16] C. Qimei, Research on Nonlinear Characteristics and Coordinated Control of MCFC-GT Hybrid System [D], Shanghai Jiaotong University doctor paper, Shanghai, 2007.
[17] C. Hitchings, Fuel Cell Handbook, sixth ed., EG&G Technical Services, Inc., Virginia, 2002.
[18] H. Morita, M. Komoda, Y. Mugikura, et al., J. Power sources 112 (2002) 509–518.
[19] P. Aguiar, C.S. Adjiman, N.P. Brandon, J. Power sources 138 (2004) 120–136.

[20] J.-H. Koh, H.-K. Seo, Y.-S. Yoo, et al., Chem. Eng. J. 87 (2002) 367–379.
[21] L. Wang, H. Zhang, S. Weng, J. Power Sources 177 (2008) 579–589.
[22] H. Zhang, S. Weng, M. Su, Dynamic Modeling and Simulation of Distributed Parameter heat Exchanger[C] Processing of ME TUBRO EXPO, Nevada, 2005, GT2005-68293.
[23] H.S. Zhang, Y.W. Liu, M. Su, S.L. Weng, Comput. Simul. 19 (2002) 79–81, in Chinese.
[24] J.S. Yang, J.L. Sohn, S.T. Ro, J. Power Sources 175 (2008) 296–302.
[25] S.H. Chan, H.K. Ho, Y. Tian, J. Power Sources 114 (2003) 213–227.